

RENDER-AND-COMPARE: CROSS-VIEW 6-DOF LOCALIZATION FROM NOISY PRIOR

Shen Yan, Xiaoya Cheng, Yuxiang Liu, Juelin Zhu, Rouwan Wu, Yu Liu*, Maojun Zhang

National University of Defense Technology

ABSTRACT

Despite the significant progress in 6-DoF visual localization, researchers are mostly driven by ground-level benchmarks. Compared with aerial oblique photography, ground-level map collection lacks scalability and complete coverage. In this work, we propose to go beyond the traditional ground-level setting and exploit the cross-view localization from aerial to ground. We solve this problem by formulating camera pose estimation as an iterative render-and-compare pipeline and enhancing the robustness through augmenting seeds from noisy initial priors. As no public dataset exists for the studied problem, we collect a new dataset that provides a variety of cross-view images from smartphones and drones and develop a semi-automatic system to acquire ground-truth poses for query images. We benchmark our method as well as several state-of-the-art baselines and demonstrate that our method outperforms other approaches by a large margin.

Index Terms— Cross-view localization, render-and-compare, aerial-to-ground dataset

1. INTRODUCTION

Visual localization aims to compute the camera pose for a given image relative to a known scene. Solving the problem is vital to many important applications, such as self-driving cars, UAV navigation, and Augmented and Virtual Reality systems.

The majority of existing image localization methods [1, 2, 3, 4, 5, 6] infer camera location and orientation using feature matching [2, 3, 4, 5] between the query image and a database of reference images from a similar perspective, usually ground-to-ground [7, 8]. The inherent limitation of these approaches is that building a complete and uniform reference map on the ground is pretty difficult and time-consuming.

Therefore, recent research [9, 10] investigates the problem of cross-view geo-localization, which localizes ground-level query images by matching them against easily accessible aerial views. However, due to a lack of reference 3D models, such methods can at most estimate a camera’s 3-DoF pose, namely, x-y coordinate position and azimuth angle. In fact, with the rapid development of 3D reconstruction techniques, it is possible to build city-scale digital twins employing aerial oblique photography, such as Google Earth. In this paper, we thus explore the possibility of utilizing aerial 3D reconstruction to

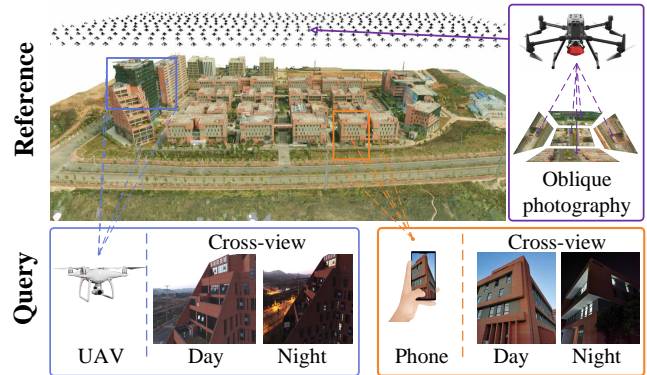


Fig. 1. Cross-view 6-DoF localization. The proposed benchmark dataset *AirLoc* exhibits drastic view changes between query and reference. The reference map is captured using a pentacular oblique camera above 100 meters, while the query images are sampled close to the ground with small drones and smartphones, respectively. Query images include real Day-and-Night environments.

conduct cross-view 6-DoF localization.

This is quite an arduous task because, unlike ground-to-ground visual localization, image retrieval and feature matching between cross-view images are inherently hard as ground-to-aerial images capture totally distinctive appearances. To solve the problem, inspired by recent view synthesis works [6], we propose a novel localization framework *Render-and-Compare*. Given an initial pose lead by the device’s sensor prior (i.e., GPS, compass, and gravity direction), our core idea is to move a virtual camera sequentially until the camera-observed scenarios align with the query image. Specifically, we first randomly sample several seeds around the sensor pose as candidates. Then, we produce synthetic images and depthmaps for all initial pose hypotheses based on textured mesh rendering. After that, we establish correspondences between the query image and synthetic candidates and select one with the largest inliers. According to pixel back-projecting in depthmap, 2D-2D correspondences can convert to 2D-3D matches, and the initial camera pose is recovered by a PnP RANSAC [11, 12]. At last, we iteratively update the former pose estimation by repeating render-and-matching operations and obtain a final result until the maximum iteration

reaches.

To the best of our knowledge, there is no public dataset for 6-DoF localization under strong viewpoint changes. To facilitate the research of this area, we collect a new benchmark dataset *AirLoc*, as shown in Figure 1. Compared with other geo-localization datasets [13, 14, 15], *AirLoc* owns the following advantages: 1) We build textured 3D mesh references based on aerial oblique photography. 2) We assign 6-DoF GT poses for query images instead of simply providing latitude, longitude, and azimuth angle. 3) The query image possesses real conditions, including significant lighting variances (e.g., Day-and-Night). 4) The query image is captured by a commonly-used cellphone or drone, rather than panoramic imaging.

We evaluate several image localization baselines and our method on the proposed dataset *AirLoc*. The experiments demonstrate that our method outperforms state-of-the-art approaches by a large margin.

In summary, our main contributions include:

- A novel render-and-compare framework for robust and accurate visual localization under significant viewpoint changes.
- A new dataset for cellphone and UAV 6-DoF localization under great viewpoint conversions and strong illumination variations.
- Benchmarking existing methods and demonstrating the effectiveness of the proposed approach.

2. RELATED WORKS

Structured localization. State-of-the-art methods [1, 2, 3, 4, 5, 6] perform visual localization by establishing 2D-3D correspondences between the query images and sparse SfM points. The camera pose is recovered using a PnP solver [12] inside a RANSAC loop [11]. Besides, an intermediate image retrieval step [16, 17] is often applied to handle large-scale problems. However, the pipeline cannot guarantee the correctness of image matching in the case of cross-view localization. In this work, we show that the render-and-compare framework enables query and reference images to share similar geometric configurations, facilitating accurate feature matching.

Geo-localization. Recently, many methods [9, 10] treat the cross-view localization problem as a standard image retrieval task and solve it by aerial-to-ground image polar transformation and global feature embedding. However, these approaches output a 3-DoF camera pose at most, which is not sufficient to support VR/AR applications on mobile devices and precise control of drones. In contrast, our method can yield 6-DoF localization under significant viewpoint changes.

Synthesis localization. Ours is not the first work to use view synthesis for visual localization. The most related to our work are [18, 6, 8]. Among them, [18] build a virtual

panoramic map in mountainous terrain, and train local features to match images and this textured mesh. However, they show pretty coarse localization (hundreds of meters level), while we achieve centimeter-accurate localization. [6] show that meshes can be used to localize images from scratch and describe a full pipeline for this task. The drawback is that they suffer from terrible feature matching under notable viewpoint changes, while our render-and-compare framework ensures high-quality image matching by providing similar perspectives. [8] render the scene from poses close to the ground-truth, and conduct iterative pose refinement for dataset GT pose labeling. We extend this idea to cross-view localization and successfully design a robust render-and-compare framework initiated from noisy sensor priors.

Localization Datasets. Almost of the existing 6-DoF localization benchmarks [7, 8] capture query and reference images from a similar perspective on the ground. The problem is that such data collection is time-consuming and cannot guarantee the integrity of the reference map. To this end, many geo-localization benchmarks are proposed recently, including CVUSA [13], CVACT [14] and VIGOR [15], which aim to determine the locations of street-view query images by matching with GPS-tagged reference images from aerial view. Although these datasets can be easily scalable to the city level, they cannot solve the 6-DoF pose due to the lack of a 3D model. We combine the advantages of the two categories datasets mentioned above and introduce a new benchmark *AirLoc*. *AirLoc* builds a large-scale 3D model via aerial oblique photography, facilitating 6-DoF visual localization of any viewpoint within the bounds of this map.

3. METHOD

Given the textured aerial reconstruction \mathcal{M} , our objective is to estimate the 6-DoF poses $\{\xi^q\}$ for the altered perspective images $\{\mathbf{I}^q\}$ based on its noisy sensor priors $\{s\xi^q\}$. We propose to tackle the cross-view issue of feature matching with a *Render-and-Compare* framework. An overview of the proposed method is exhibited in Figure 2.

3.1. Prior Pose Generation

The sensor pose acquisition for mobile phones can be divided into two parts: 1) For translation, we apply latitude and longitude coordinates in GPS as an x-y value. Due to the low accuracy of GPS along altitude direction, we vertically project the x-y position onto the pre-build 3D surface and record its floor height. We then plus 1.5 meters upon the floor to obtain the z value, as phone photos are generally taken with a hand-held gesture. 2) For rotation, we build $SO(3)$ matrix utilizing gravity and compass direction from mobile sensor.

Considering the sensor noises on the ground, we augment pose perturbations for UAVs and smartphones. Specifically, we extend ± 5 meters for x-y coordinate and supplement ± 60

degrees for Euler angle yaw around the pose prior. We only adjust the yaw angle because the gravity sensor, which determines roll and pitch angles, shows high accuracy. The candidates of initial pose increase from ${}_s\xi^q$ to $\{{}_s\xi_1^q, \dots, {}_s\xi_k^q\}$, where k is the augment number.

3.2. View Synthesis

For a query \mathbf{I}^q , assuming that we have obtained all possible initials $\{{}_s\xi_1^q, \dots, {}_s\xi_k^q\}$, we aim to acquire the corresponding textured renderings and depthmaps. Taking the time overhead into account, we apply Workbench Engine in Blender¹ with flat color mechanisms for fast rendering. Note that although we now use Blender to verify the *Render-and-Compare* framework, the pipeline can be replaced with a more advanced rendering technique, such as Neural Radiance Field (NeRF) [19]. We denote the rendered image and depth for each virtual pose ${}_s\xi_i^q$ as $({}_s\mathbf{I}_i^q, {}_s\mathbf{d}_i^q)$.

3.3. Pose Correction

The pose correction stage first selects the maximum likelihood pose $\xi_{t_1}^q$ from initial candidates $\{{}_s\xi_1^q, \dots, {}_s\xi_k^q\}$. In detail, we employ state-of-the-art learned local features [2] and matching strategies [3, 4] to find 2D-2D correspondences between query \mathbf{I}^q and renderings $\{{}_s\mathbf{I}_i^q | i = 1, \dots, k\}$, where k is the seed number. A fundamental matrix is employed to prune possible incorrect correspondences. The candidate with the largest matching number wins the selection, and $(\xi_{t_0}^q, \mathbf{I}_{t_0}^q, \mathbf{d}_{t_0}^q)$ is regarded as the first (t_0) iteration during pose correction. Then, we lift 2D-2D to 2D-3D matches using current pose estimation $\xi_{t_0}^q$ and the depth map $\mathbf{d}_{t_0}^q$. The next pose estimation $\xi_{t_1}^q$ is recovered by a P3P solver [12] within LO-RANSAC [11] loops. We repeat the iterative camera optimizations by h times. Finally, the computed pose converges to an ultimate result $\xi^q = \xi_{t_h}^q$. Taking efficiency and effectiveness into consideration, we set $k = 15, h = 3$ in the experiment.

4. DATASET

The released dataset *AirLoc* includes a large urban area (approximately $100,000m^2$), containing buildings, streets, and vegetation. In total, there are 1,970 reference images and 1,432 query images. The query images are captured from various viewpoints, including smartphones on the ground and UAVs in the near air. Moreover, the query images incorporate Day-and-Night conditions. Please see Figure 1 for a visualization of the dataset.

4.1. Reference Map Collection

We capture high-resolution aerial image sequences with a five-eye oblique camera on a flight platform, using SHARE PSDK

¹<https://www.blender.org>

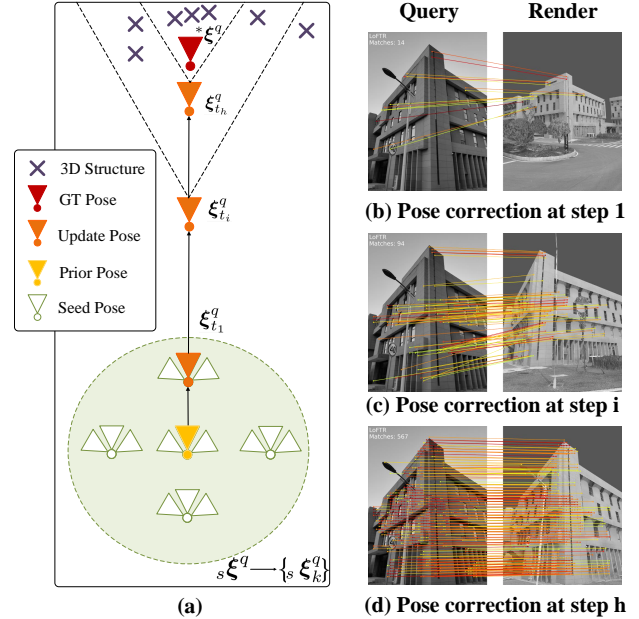


Fig. 2. Overview of the proposed method. (a). For each prior pose ${}_s\xi^q$, we first eliminate the noise by adding several random seeds $\{{}_s\xi_1^q, \dots, {}_s\xi_k^q\}$. Then we choose one by calculating the maximum inlier matching number as $\xi_{t_1}^q$. The virtual pose experiences a render-and-compare update process towards GT target ξ^q , varies from intermediate $\xi_{t_i}^q$ at step i to final $\xi_{t_h}^q$ at step h . (b,c,d). The feature correspondences are visualized between the query and rendered image during the iterative refinement, where warmer colors indicate higher confidence. The matching results improve a lot along with the sequential adjustments.

102S² and DJI M300 RTK³, respectively. In order to fully and evenly cover the survey area, all flight paths are pre-planned in a grid fashion and automated by the flight control system supported by DJI M300. We apply modern 3D reconstruction techniques to build a textured mesh model and align it with the real geographic world with built-in RTK measurements. Note that, the camera has the ability to take both oblique and nadir photographs, ensuring that vertical surfaces are captured appropriately. Please refer to the supplementary material for a more detailed introduction.

4.2. Query Image Collection

We conduct query image acquisition using smartphones and a micro aerial vehicle, including HUAWEI Mate30 and DJI Phantom 4⁴. The query images include multiple sessions during daytime and night-time. For each session, we use

²<https://www.shareuavtec.com/ProductDetail/6519312.html>

³<https://www.dji.com/cn/matrice-300>

⁴<https://www.dji.com/cn/phantom-4-pro>

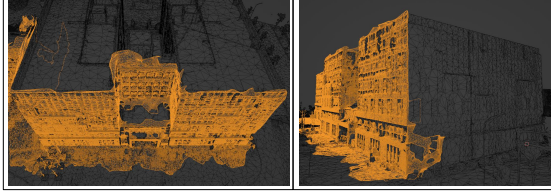


Fig. 3. Alignment quality of the aerial-to-ground reconstruction on *AirLoc*. The dark black model comes from aerial oblique photography, while the yellow model is built from a sequence of ground cellphone photos. The accuracy of the alignment can be observed in, for instance, the agreement of corners and edges.

SensorLog Application⁵ to record raw in-build data. Since our method studies robust visual localization under noisy priors, we do not ensure the hardware is synchronized and carefully calibrated for all sensors. More details are provided in the supplementary material.

4.3. Query GT Generation

We apply a scalable semi-automatic annotation to find the GT pose parameters $\{\xi_i^q\}$ for query images. Our GT tool can label thousands of query poses, while only asking for dozens of manual assignments. In detail, we first employ Structure-from-Motion to reconstruct sparse point clouds for reference images and multiple query sequences, respectively. As ground and aerial images show remarkable visual differences, it is quite difficult to match keypoints even adopting state-of-the-art learning-based techniques [3, 4]. We then manually specify some iconic tie points across aerial-and-ground images, and conduct bundle adjustment for all individual SfM blocks. Finally, we obtain an integral 3D registration model, which owns camera poses for reference and query images. We evaluate the accuracy of the GT poses by median reprojection errors, which are 0.52 pixels for the whole 3D model and 0.38 for tie points. For visual inspection, we demonstrate the aerial and ground model registration quality in Figure 3. Besides, we randomly render images at the estimated GT poses using the textured mesh in Figure 4. They appear in pixel-level alignment, supporting that the poses are accurate.

5. EXPERIMENT

In this section, we introduce the selection of baselines and evaluation metrics on *AirLoc* dataset in Section 5.1. Experimental results and ablation studies are reported in Section 5.2 and Section 5.3, respectively.

⁵<http://sensorlog.berndthomas.net>

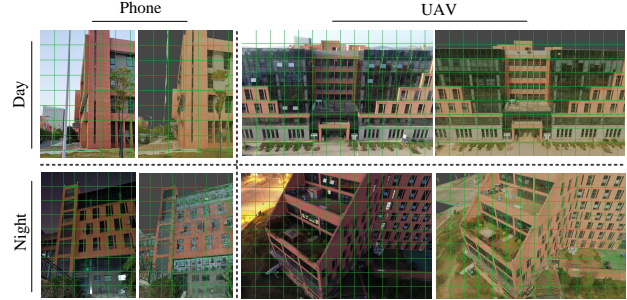


Fig. 4. GT poses quality on *AirLoc*. Pixel-aligned renderings of the estimated camera pose confirm that the poses are sufficiently accurate for our evaluation.

5.1. Baselines and Metrics

Baselines. We compare our approach with state-of-the-art visual localization baselines, mainly HLoc [1, 3] and MeshLoc [6], with different feature extractors and matchers, including sparse keypoint-based methods (SIFT [20], SuperPoint(SPP) [2], Nearest Neighbors(NN), SuperGlue(SPG) [3]) and semi-dense methods (LoFTR [4], Patch2Pix [5]). For our render-and-compare framework, we adopt SuperPoint(SPP) [2]+SuperGlue(SPG) [3] and LoFTR [4] to match query images and virtual renderings. Note that all mentioned features are directly applied without fine-tuning or re-training on the *AirLoc* dataset.

For a fair comparison, we do not employ global features to retrieve image pairs for HLoc and MeshLoc, as we found that feature-based approaches (e.g., NetVLAD [16]) suffered a lot in cross-view situations. Instead, We first obtain top-50 retrieval pairs by computing a modified Chamfer distance between prior observed points of the query and 3D observation of the reference. Then, we exploit the compass direction and GPS x-y coordinates to filter obvious wrong ranks. Supplemental materials provide more details.

Metrics. We follow the standard localization evaluation procedure [7], and report the localization recall at thresholds $(25cm, 2^\circ)$, $(50cm, 5^\circ)$, and $(1m, 10^\circ)$. We divide the results into four splits by Day-and-Night conditions and different capturing devices.

5.2. Evaluation Results and Analysis

The localization results are reported in Table 1. Our method substantially outperforms HLoc [1, 3] and MeshLoc [6] by a large margin under all conditions, even we employ the same local features (e.g., SuperPoint(SPP) [2]+SuperGlue(SPG) [3] and LoFTR [4]). The results fully demonstrate the capability of our render-and-compare design for camera localization.

We attribute the success to the following mechanism: feature matching between real-to-render pairs with similar viewpoints owns overwhelming advantages over read-to-real

Method	Day		Night	
	(25cm, 2°) / (50cm, 5°) / (1m, 10°)			
UAV				
HLoc (<i>SIFT + NN</i>)	19.8 / 31.5 / 37.0	5.2 / 62.6 / 80.0		
HLoc (<i>SPP + NN</i>)	41.6 / 52.9 / 56.3	0.0 / 29.6 / 87.8		
HLoc (<i>SPP + SPG</i>)	67.2 / 84.9 / 87.4	0.0 / 53.9 / 100.0		
MeshLoc (<i>SPP + NN</i>)	14.7 / 31.5 / 46.6	1.7 / 29.6 / 60.9		
MeshLoc (<i>Patch2Pix</i>)	19.3 / 34.5 / 48.7	1.7 / 23.5 / 58.3		
MeshLoc (<i>SPP + SPG</i>)	72.7 / 80.0 / 82.8	0.0 / 69.6 / 98.3		
MeshLoc (<i>LoFTR</i>)	74.0 / 83.6 / 84.5	0.0 / 40.9 / 90.4		
Ours (<i>SPP + SPG</i>)	90.8 / 99.6 / 100.0	90.0 / 100.0 / 100.0		
Ours (<i>LoFTR</i>)	84.5 / 99.6 / 100.0	81.7 / 99.1 / 100.0		
Phone				
HLoc (<i>SIFT + NN</i>)	0.0 / 0.0 / 0.0	0.0 / 0.0 / 0.0		
HLoc (<i>SPP + NN</i>)	0.0 / 0.0 / 0.0	0.0 / 0.0 / 0.0		
HLoc (<i>SPP + SPG</i>)	19.1 / 25.3 / 28.3	19.1 / 25.1 / 27.8		
MeshLoc (<i>SPP + NN</i>)	0.0 / 0.0 / 0.0	0.0 / 0.0 / 0.2		
MeshLoc (<i>Patch2Pix</i>)	0.0 / 0.0 / 0.0	0.0 / 0.0 / 0.6		
MeshLoc (<i>SPP + SPG</i>)	14.5 / 22.8 / 26.9	10.7 / 12.9 / 15.9		
MeshLoc (<i>LoFTR</i>)	12.1 / 18.3 / 22.2	11.1 / 15.3 / 18.6		
Ours (<i>SPP + SPG</i>)	47.8 / 81.0 / 86.1	24.5 / 56.2 / 68.6		
Ours (<i>LoFTR</i>)	46.5 / 81.6 / 88.9	28.2 / 60.7 / 74.4		

Table 1. Visual localization results. We report the recall at (25cm,2deg) / (50cm,5deg) / (1m,10deg). Our method is compared with HLoc [1] and MeshLoc [6] with different feature-matching methods.

pairs with distinct perspectives. To visually explain this phenomenon, we provide the LoFTR [4] feature-matching results in Figure 5. It is obvious that close synthetic view local matching takes the lead in terms of accuracy and number.

5.3. Ablation Studies

Iteration number. As a sequential update method, we exploit the influence of the iteration number. Increasing the number increases the localization at all thresholds, as reported in Table 2. Considering that well-matured OpenGL-based rendering technology, which is optimized for real-time performance on GPUs [6], this render-and-compare solution has the potential to efficiently achieve better results with more refinements.

Seed initialization. We evaluate the effect with or without translation and rotation augmentations of the initialization. As shown in Table 3, both parameters significantly influence the final localization accuracy, especially for the phone data split, which proves the effectiveness of the proposed initial pose enhancement strategy.

6. CONCLUSION

In this paper, we present a new approach for cross-view 6-DoF localization from noisy priors. To overcome the difficulties of image matching over distinctive viewpoints, we propose a render-and-compare framework to sequentially refine the pose

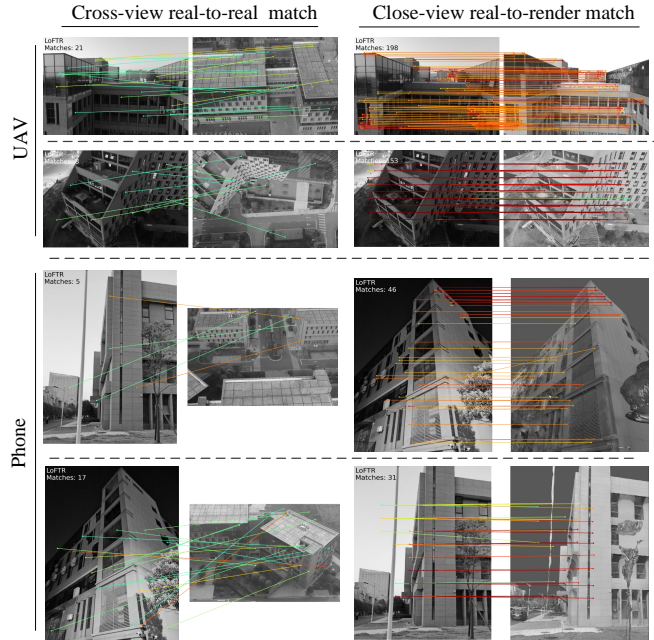


Fig. 5. Mechanism analysis of advantage of our method. The left column shows that state-of-the-art learned feature LoFTR [4] cannot establish correspondences for real image pairs sharing notable viewpoint differences. The right column illuminates that LoFTR [4] is good at matching real-and-synthetic views with similar poses. Warmer colors show higher confidence.

estimation. The localization performance is evaluated on a new aerial-to-ground dataset with an oblique photography map. Our results demonstrate significant improvements compared to state-of-the-art localization methods.

7. REFERENCES

- [1] Paul-Edouard Sarlin, Cesar Cadena, Roland Siegwart, and Marcin Dymczyk, “From coarse to fine: Robust hierarchical localization at large scale,” in *Proceedings of the IEEE/CVF Conference on Computer Vision and Pattern Recognition*, 2019, pp. 12716–12725.
- [2] Daniel DeTone, Tomasz Malisiewicz, and Andrew Rabinovich, “Superpoint: Self-supervised interest point detection and description,” in *Proceedings of the IEEE conference on computer vision and pattern recognition workshops*, 2018, pp. 224–236.
- [3] Paul-Edouard Sarlin, Daniel DeTone, Tomasz Malisiewicz, and Andrew Rabinovich, “Superglue: Learning feature matching with graph neural networks,” in *Proceedings of the IEEE/CVF conference on computer vision and pattern recognition*, 2020, pp. 4938–4947.
- [4] Jiaming Sun, Zehong Shen, Yuang Wang, Hujun Bao, and Xiaowei Zhou, “Loftr: Detector-free local feature

Method	Day	Night
	(25cm, 2°) / (50cm, 5°) / (1m, 10°)	
UAV		
LoFTR (iter 1)	73.1 / 98.3 / 100.0	47.8 / 81.7 / 96.5
LoFTR (iter 2)	75.2 / 99.4 / 100.0	79.1 / 96.5 / 99.1
LoFTR (iter 3)	84.5 / 99.6 / 100.0	81.7 / 99.1 / 100.0
SPP+SPG (iter 1)	82.3 / 99.2 / 100.0	89.6 / 100.0 / 100.0
SPP+SPG (iter 2)	84.9 / 99.6 / 100.0	89.7 / 100.0 / 100.0
SPP+SPG (iter 3)	90.8 / 99.6 / 100.0	90.0 / 100.0 / 100.0
Phone		
LoFTR (iter 1)	12.6 / 37.7 / 68.3	5.3 / 20.5 / 46.4
LoFTR (iter 2)	37.3 / 75.4 / 86.9	17.6 / 50.1 / 65.5
LoFTR (iter 3)	46.5 / 81.6 / 88.9	28.2 / 60.7 / 74.4
SPP+SPG (iter 1)	12.0 / 36.0 / 67.4	3.8 / 14.1 / 39.3
SPP+SPG (iter 2)	37.0 / 73.6 / 84.1	15.2 / 43.1 / 58.2
SPP+SPG (iter 3)	47.8 / 81.0 / 86.1	24.5 / 56.2 / 68.6

Table 2. Ablation studies. Different iteration number {1, 2, 3} in our render-and-compare framework is compared with (25cm,2deg) / (50cm,5deg) / (1m,10deg) metrics.

Initial augmentation	Day	Night
	(25cm, 2°) / (50cm, 5°) / (1m, 10°)	
UAV		
Seed (not used)	81.9 / 98.3 / 100.0	79.1 / 96.5 / 99.1
Seed (translation x-y)	81.9 / 99.6 / 100.0	79.1 / 96.5 / 100.0
Seed (rotation yaw)	81.9 / 99.2 / 100.0	81.7 / 99.1 / 100.0
Seed (both)	84.5 / 99.6 / 100.0	81.7 / 99.1 / 100.0
Phone		
Seed (not used)	5.8 / 16.3 / 35.1	9.1 / 28.5 / 38.6
Seed (translation x-y)	36.8 / 46.5 / 68.5	18.3 / 46.8 / 58.3
Seed (rotation yaw)	34.1 / 65.3 / 72.6	21.3 / 44.3 / 60.0
Seed (both)	46.5 / 81.6 / 88.9	28.2 / 60.7 / 74.4

Table 3. Ablation studies. Different seed augmentation strategies are compared with (25cm,2deg) / (50cm,5deg) / (1m,10deg) metrics using LoFTR [4].

matching with transformers,” in *Proceedings of the IEEE/CVF conference on computer vision and pattern recognition*, 2021, pp. 8922–8931.

- [5] Qunjie Zhou, Torsten Sattler, and Laura Leal-Taixe, “Patch2pix: Epipolar-guided pixel-level correspondences,” in *Proceedings of the IEEE/CVF conference on computer vision and pattern recognition*, 2021, pp. 4669–4678.
- [6] Vojtech Panek, Zuzana Kukelova, and Torsten Sattler, “Meshloc: Mesh-based visual localization,” in *European Conference on Computer Vision*. Springer, 2022, pp. 589–609.
- [7] Torsten Sattler, Will Maddern, Carl Toft, Akihiko Torii, Lars Hammarstrand, Erik Stenborg, Daniel Safari, Masatoshi Okutomi, Marc Pollefeys, Josef Sivic, et al., “Benchmarking 6dof outdoor visual localization in changing conditions,” in *Proceedings of the IEEE*

conference on computer vision and pattern recognition, 2018, pp. 8601–8610.

- [8] Zichao Zhang, Torsten Sattler, and Davide Scaramuzza, “Reference pose generation for long-term visual localization via learned features and view synthesis,” *International Journal of Computer Vision*, vol. 129, no. 4, pp. 821–844, 2021.
- [9] Yujiao Shi, Liu Liu, Xin Yu, and Hongdong Li, “Spatial-aware feature aggregation for image based cross-view geo-localization,” *Advances in Neural Information Processing Systems*, vol. 32, 2019.
- [10] Hongji Yang, Xiufan Lu, and Yingying Zhu, “Cross-view geo-localization with layer-to-layer transformer,” *Advances in Neural Information Processing Systems*, vol. 34, pp. 29009–29020, 2021.
- [11] Ondřej Chum, Jiří Matas, and Josef Kittler, “Locally optimized ransac,” in *Joint Pattern Recognition Symposium*. Springer, 2003, pp. 236–243.
- [12] Bert M Haralick, Chung-Nan Lee, Karsten Ottenberg, and Michael Nölle, “Review and analysis of solutions of the three point perspective pose estimation problem,” *International journal of computer vision*, vol. 13, no. 3, pp. 331–356, 1994.
- [13] Menghua Zhai, Zachary Bessinger, Scott Workman, and Nathan Jacobs, “Predicting ground-level scene layout from aerial imagery,” in *Proceedings of the IEEE Conference on Computer Vision and Pattern Recognition*, 2017, pp. 867–875.
- [14] Liu Liu and Hongdong Li, “Lending orientation to neural networks for cross-view geo-localization,” in *Proceedings of the IEEE/CVF Conference on Computer Vision and Pattern Recognition*, 2019, pp. 5624–5633.
- [15] Sijie Zhu, Taojiannan Yang, and Chen Chen, “Vigor: Cross-view image geo-localization beyond one-to-one retrieval,” in *Proceedings of the IEEE/CVF Conference on Computer Vision and Pattern Recognition*, 2021, pp. 3640–3649.
- [16] Relja Arandjelovic, Petr Gronat, Akihiko Torii, Tomas Pajdla, and Josef Sivic, “Netvlad: Cnn architecture for weakly supervised place recognition,” in *Proceedings of the IEEE conference on computer vision and pattern recognition*, 2016, pp. 5297–5307.
- [17] Shen Yan, Maojun Zhang, Shiming Lai, Yu Liu, and Yang Peng, “Image retrieval for structure-from-motion via graph convolutional network,” *Information Sciences*, vol. 573, pp. 20–36, 2021.
- [18] Jan Brejcha, Michal Lukáč, Yannick Hold-Geoffroy, Oliver Wang, and Martin Čadík, “Landscapear: Large scale outdoor augmented reality by matching photographs with terrain models using learned descriptors,” in *European Conference on Computer Vision*. Springer, 2020, pp. 295–312.
- [19] Haithem Turki, Deva Ramanan, and Mahadev Satyanarayanan, “Mega-nerf: Scalable construction of large-

scale nerfs for virtual fly-throughs,” in *Proceedings of the IEEE/CVF Conference on Computer Vision and Pattern Recognition*, 2022, pp. 12922–12931.

- [20] David G Lowe, “Distinctive image features from scale-invariant keypoints,” *International journal of computer vision*, vol. 60, no. 2, pp. 91–110, 2004.